

Peratic Phase Transition by Bulk-to-Surface Response

Xingze Qiu,^{1,2} Hai Wang,^{1,2} Wei Xia,¹ and Xiaopeng Li^{1,2,*}

¹State Key Laboratory of Surface Physics, Institute of Nanoelectronics and Quantum Computing,
and Department of Physics, Fudan University, Shanghai 200438, China

²Shanghai Qi Zhi Institute, Shanghai 200030, China

(Dated: September 29, 2021)

The study of phase transitions in ground states or thermal equilibrium is at the heart of statistical physics. The well established scenarios are Landau spontaneous symmetry breaking and topological ordering, the former characterized by a local order parameter, and the latter by state topology that typically comes with protected surface modes by the bulk-edge correspondence. Here, we provide a scenario beyond these conventional paradigms, and show the bulk-to-surface response defines a novel phase transition in the ground state, dubbed “peratic”, meaning defined by the boundary. This phase transition arises in both classical and quantum many-body systems. We construct frustration free Hamiltonians and show rigorously that a time-like dimension emerges in their static ground states, by which our peratic phase transition has an exact duality to chaotic phase transitions in dynamical systems. The quantum ground state is a superposition of geometrical lines on a two dimensional array. Our prediction has direct consequences in quantum simulation platforms such as Rydberg atoms and superconducting qubits, as well as anisotropic spin glass materials. The discovery would shed light on the unification of dynamical phase transitions with equilibrium systems.

Characterization of different phases of matter is fundamental to our understanding of nature. Despite the complexity of various phases of matter existent in nature, progress has been made from the aspects of symmetry and topology. A broad range of thermal equilibrium or ground state phase transitions such as crystallization, superfluidity, and magnetism, has been framed by Landau’s spontaneous symmetry breaking theory, where different phases are characterized by local order parameters of different symmetry representations [1]. The long-wavelength properties of the resultant symmetry broken phases are described by corresponding effective field theories [2]. More recent research efforts have been devoted to topological phases in quantum ground state matters [3–5]. The topological phases in absence of local order parameters are instead characterized by topologically quantized invariants, with their physical properties described by topological quantum field theories, where nontrivial protected surface effects arise from the bulk-edge correspondence. This has led to a generic scenario beyond Landau’s spontaneous symmetry breaking paradigm in classification of phases of matter.

In pursuing unconventional phases, quantum many-body states far away from equilibrium have also attracted much present research interest. Non-equilibrium many-body physics previously unreachable can now be probed in experimental systems such as light-driven electronic matters [6] and highly controllable quantum simulation [7–10] or quantum computing platforms [11–14]. Quantum many-body localization happens for a disorder system in its dynamical properties at infinite temperature [15, 16]. Anomalous protected edge modes at zero Chern number which are unexpected for equilibrium systems, could appear in periodically driven Floquet quantum dynamics [17–19]. Spontaneous translation symmetry breaking is generalized to the temporal domain, giving rise to crystallization in time [10, 11, 20–23]. There is mounting evidence suggesting non-equilibrium phases may contain exotic scenarios beyond equilibrium setups.

Here, we report a hitherto unheardof phase transition mechanism—bulk-to-surface (BTS) response defines a phase transition in Hamiltonian ground states, reaching beyond the known paradigms. We establish this mechanism by constructing frustration free Hamiltonians in both classical and quantum settings, and show rigorously how a time-like dimension emerges in their static ground states. The ground states have two distinctive phases as determined by whether the bulk is rigid against manipulations at the surface. The phase transition is characterized by a BTS response

$$\chi_{\text{BTS}} = \text{Var}(\langle O_{\text{bulk}} \rangle) |_{\text{surface manipulation}} \quad (1)$$

being zero or finite, with $\langle O_{\text{bulk}} \rangle$ an observable in the bulk, $\text{Var}(\langle O_{\text{bulk}} \rangle)$ the variance of the bulk observable as we manipulate the surface. The BTS response quantifies the stability of the bulk against surface manipulations, which vanishes if the bulk is stable and acquires a finite value otherwise. The phase transition in the classical ground state has an exact duality to the order-to-chaos transition in classical nonlinear dynamical systems [24]. The quantum ground state phase transition constructed by forming quantum superposition of fluctuating line configurations has a rigorous duality with the quantum ergodic [25–27] to many-body-localization (MBL) phase transition [15, 16] in quantum many-body dynamics. Our theory implies that the study of unconventional phases in non-equilibrium systems would rather inspire discovery of more exotic equilibrium phases and transitions than reaching beyond.

Emergent chaotic dynamics in a Hamiltonian ground state.— We first consider a discrete classical system which contains binary degrees of freedom $z_{ij} = \pm 1$ on a two dimensional (2d) grid, with the indices $i \in [0, I-1]$, and $j \in [0, J-1]$. Our theory starts from constructing a Hamiltonian ground state that supports the phase transition scenario described by the BTS response in Eq. (1). The Hamiltonian contains a bulk

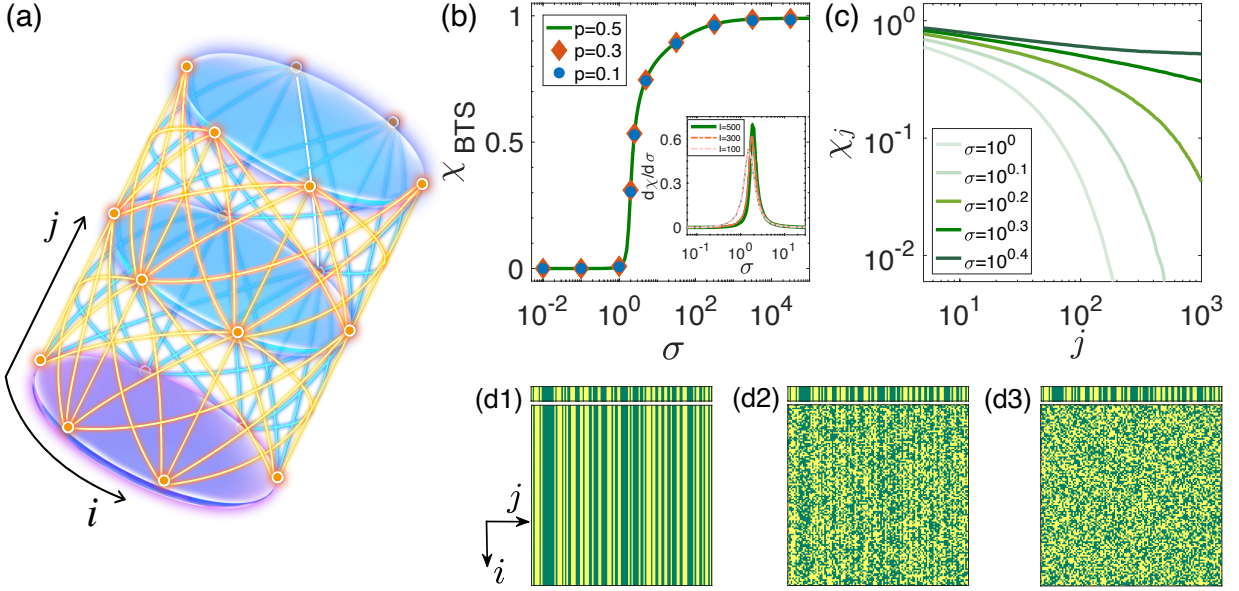


FIG. 1. Classical peratic phase transition. (a), illustration of the couplings of the model in Eq. (3) with an interaction range $M = 2$. (b), the BTS response (χ_{BTS}) across the phase transition for $I = 500$. It vanishes at small coupling variance (σ) and becomes finite across the phase transition. The BTS response is averaged over random surface terms (h_{surf}), with p the probability of each surface term $h_{\text{surf},i}$ taking a positive value. The inset of (b) shows its first derivative for $I = 100, 300, 500$ with $p = 0.5$. This derivative develops a peak near the transition point, which sharpens up as we increase the system size. This implies a divergent second derivative in the thermodynamic limit. (c), the dependence of local BTS response (χ_j) on the j index. This quantity has an exponential decay at small σ when χ_{BTS} vanishes. The decay becomes power law at the critical point (σ_c). (d), typical configurations of z_{ij} in three different regimes $\sigma \ll \sigma_c$, $\sigma \approx \sigma_c$, and $\sigma \gg \sigma_c$, from left to right. In this plot, we fix $J = 5I$, and sample over different Hamiltonian realizations, namely W_{ij} , and u_j .

and a surface term, H_{bulk} , and H_{surface} ,

$$\begin{aligned}
 H_{\text{bulk}} &= - \sum_i \sum_{j>0} z_{ij} \text{sgn} \left[u_j + \sum_{m=-M}^M w_m^{[ij]} z_{i+m, j-1} \right], \\
 H_{\text{surf}} &= - \sum_i h_{\text{surf}}^{[i]} z_{i,0},
 \end{aligned} \quad (2)$$

where $w^{[ij]}$ represents Ising couplings, u_j is a local field in the bulk, and $h_{\text{surf}}^{[i]}$ is a local field on the surface introduced to study the BTS response. The Ising couplings are randomly drawn from a Gaussian distribution with zero mean and variance σ^2 . The bulk local field u_j takes random binary values ± 1 with equal probability. We adopt an open boundary condition along the j -axis and periodic boundary along the other axis (Fig. 1). The system has a layer structure along the j -axis—we have inter-layer couplings only.

Minimizing each term of the Hamiltonian in Eq. (2) leads to a set of equations,

$$z_{i0}^g = \text{sgn}(h_{\text{surf}}^{[i]}), \quad z_{i,j>0}^g = \text{sgn} \left(u_j + \sum_{m=-2}^2 w_m^{[ij]} z_{i+m, j-1}^g \right), \quad (3)$$

which can all be satisfied. The Hamiltonian is thus frustration free. The binary degrees of freedom in the Hamiltonian ground state is given by z_{ij}^g . We then observe that the j -dependence of the binary variables in the static ground state is time-like, for the j -th layer is completely determined by the

$(j-1)$ -th layer. A time-like dimension thus arises in the static ground state.

By treating the j -axis as a time evolution direction, Eq. (3) maps onto classical nonlinear dynamics having an order-to-chaos dynamical phase transition [24]. In the ordered phase ($\sigma < \sigma_c$), the dynamical state is pinned by the local field u_j —the difference between two initial states as measured by Hamming distance is quickly washed away in the dynamical evolution. In the chaotic phase ($\sigma > \sigma_c$), the difference in the initial states would either remain or gain amplification by the nonlinear dynamics. Consequently, the ground state of the Hamiltonian in Eq. (2) also has two phases. For $\sigma < \sigma_c$, the system is in a rigid phase where the bulk is stable and immune to surface manipulations with different h_{surf} . For $\sigma > \sigma_c$, we have a volatile phase with the bulk sensitive to surface manipulations. Quantitatively, the BTS response for this specific system is defined as

$$\chi_{\text{BTS}} = \lim_{h_{\text{surf}} \rightarrow 0} \left[\frac{1}{IJ} \sum_{ij} \text{Var}(z_{ij}) |h_{\text{surf}} \right], \quad (4)$$

with the variance taken by randomly sampling h_{surf} . We also introduce a space resolved local BTS response $\chi_j = I^{-1} \sum_i \text{Var}(z_{ij}) |h_{\text{surf}}$ to diagnose the phase transition criticality. Their behavior across the phase transition is shown in Fig. 1. The BTS response vanishes in the rigid phase, and becomes finite in the volatile phase, defining our peratic phase transition. By increasing the system size, we find the BTS response

has a divergent second derivative at the critical point. The local BTS response shows an exponential decay in the rigid phase, with a decay length that tends to diverge approaching the critical point. At the critical point, the local BTS response exhibits a power law scaling, $\chi_j \propto j^{-\eta}$, a signature of non-trivial criticality for the peratic phase transition. We argue the critical behavior is described by a universal finite size scaling function

$$\chi_{\text{BTS}}(t, L) = L^{-\eta} G(Lt^\nu), \quad (5)$$

with $I, J \propto L$, $t = (\sigma - \sigma_c)/\sigma_c$, and determine the anomalous dimension $\eta = 0.172(2)$, and ν -exponent $\nu = 2.73(8)$ (*Supplementary Materials*). This phase transition scenario does not rely on the symmetry or the topology of the system, and thus goes beyond the conventional phase transition paradigms.

One fascinating property of the volatile phase is its robustness—the BTS response is stable irrespective of different choices of surface manipulations. In our numerical calculation, each surface term $h_{\text{surf},i}$ takes a positive value with a probability p , and a negative value with $1 - p$. The BTS response in the volatile phase as constructed above does not vary with the p -value (Fig. 1(b)), i.e., having robustness against different surface manipulations. This nontrivial property can be attributed to the presence of a dynamical fixed point of the Hamming distance evolution in the dual chaotic dynamics [28]. This makes the volatile phase sharply distinctive from a trivial case with the bulk trivially determined by the surface, for example with $z_{ij} = z_{i0}$, where the BTS response would strongly depend on p .

Experimental candidates.— Although the frustration free Hamiltonian in Eq. (2) has a nice property of being polynomially solvable, it contains high-order interactions, whose corresponding experimental systems are rare. We further consider a Hamiltonian with two-body Ising couplings only,

$$H_{\text{bulk}} = - \sum_i \sum_{j>0} z_{ij} \left[u_j + \sum_{m=-M}^M w_m^{[ij]} z_{i+m,j-1} \right], \quad (6)$$

which could describe a broad range of spin systems from Rydberg atomic systems [29] and superconducting qubits [30] to anisotropic spin glasses [31]. Furthermore, it is natural to generalize Eq. (6) to quantum systems, by simply promoting the Ising variables z_{ij} to Pauli operators \hat{z}_{ij} , and adding a transverse field coupling $\Delta H = \sum_{ij} h_T \hat{x}_{ij}$ (\hat{x} the Pauli-x operator) to generate quantum fluctuations. These Hamiltonians are no longer frustration free. We then study their ground state phase transition by numerically minimizing the energy. We find that the BTS responses for the frustrated and frustration-free models are quite similar to each other with a tiny difference barely noticeable (*Supplementary Materials*). The peratic phase transition still preserves in the frustrated model. As a specific example, we have considered a system of Rydberg p-wave dressed atoms (*Supplementary Materials*), whose description closely resembles Eq. (6), and predict this system indeed has a peratic phase transition (*Supplementary Fig. S3*).

Quantum peratic phase transition.— For the numerical calculation of the quantum ground state of the transverse field Ising model is limited in the system size, we further construct a quantum peratic phase transition characterized by the BTS response, that has an exact duality with the quantum MBL transition of the one-dimensional Floquet quantum dynamics of a disordered spin chain [15, 16]. Since the existence of the MBL transition has been mathematically proven for one-dimensional systems by Imbrie [32], our construction provides a rigorous scenario for the quantum peratic phase transition.

We consider a 2d qudit lattice system with a four dimensional local Hilbert space. The four levels are labeled as $\begin{pmatrix} v \\ z \end{pmatrix}$ with $v (= 0, 1)$ and $z (= \pm 1)$. The lattice contains I rows and J rungs, with two types of rungs labeled by A and B (see Fig. 2(a)). Different qudits are labeled according to their position on the lattice by (i, j) , with $i \in [0, I-1]$ and $j \in [0, J-1]$.

The large 4^{IJ} -dimensional Hilbert space of the qudit system is projected to a legal subspace with a dimension $IJ \times 2^I$ (*Supplementary Materials*). The legal quantum states are illustrated in Fig. 2(a), which are represented by two types of lines—Type A and Type B . Type A (B) line starts from the bottom (top) at A (B) sites, goes straight upward (downward), bends at most once to the right, and then runs upward (downward) following the B (A) rungs to the top (bottom). We have a total number of IJ lines, with each line uniquely labeled by (i, j) , according to the site where the line bends over, or the last site if the line does not bend. The quantum state on the line is assumed to be $\begin{pmatrix} 1 & 1 & \dots & 1 \\ z_0 & z_1 & \dots & z_{I-1} \end{pmatrix}$, with the subscripts labeled by the order from top to bottom on the lattice. The qudits to its left (right) all reside on the state $\begin{pmatrix} 0 \\ -1 \end{pmatrix} \left(\begin{pmatrix} 0 \\ 1 \end{pmatrix} \right)$. All the legal states can then be labeled as $|i, j; \vec{z}\rangle$ [$\vec{z} \equiv (z_0, z_1 \dots z_{I-1})$]. We introduce a sequential index, l , for a compact representation of (i, j) — $l_{ij} = jI + i$ for $j \in A$, and $l_{ij} = (j+1)I - i - 1$ for $j \in B$.

We construct a 2d local qudit Hamiltonian (*Supplementary Materials*), whose projection on the legal subspace gives an effective Hamiltonian

$$H_{\text{eff}} = \sum_{\vec{z}_*} \left\{ -\frac{1}{2} (|\gamma_0(\vec{z}_*)\rangle\langle\gamma_0(\vec{z}_*)| - |\gamma_{IJ-1}(\vec{z}_*)\rangle\langle\gamma_{IJ-1}(\vec{z}_*)|) + \sum_{l=0}^{IJ-2} \frac{1}{2} (|\gamma_l(\vec{z}_*)\rangle\langle\gamma_l(\vec{z}_*)| - |\gamma_l(\vec{z}_*)\rangle\langle\gamma_{l+1}(\vec{z}_*)| + H.c.) \right\}. \quad (7)$$

Here, the γ -states take a form $|\gamma_l(\vec{z}_*)\rangle = \sum_{\vec{z}} \psi_l(\vec{z}) |l; \vec{z}\rangle$. The wave functions $\psi_l(\vec{z})$ are defined through a sequential unitary transformation starting from $\psi_0(\vec{z}) = \delta_{\vec{z}, \vec{z}_*}$. The update of ψ_l is designed to follow the Floquet quantum dynamics of a one-dimensional spin-1/2 system [33]. From $l = 0$ to $l = I-1$, the update of ψ_l corresponds to a unitary gate $e^{-i\hat{x}_i \hat{x}_{i+1}/10}$ (i from 0 to $I-1$), and these unitary gates are then applied in a backward order from $l = I$ to $2I-1$. Then in the same order, we apply the unitary gates $e^{-i\hat{y}_i \hat{y}_{i+1}/10}$ from $l = 2I$ to $l = 4I-1$, and

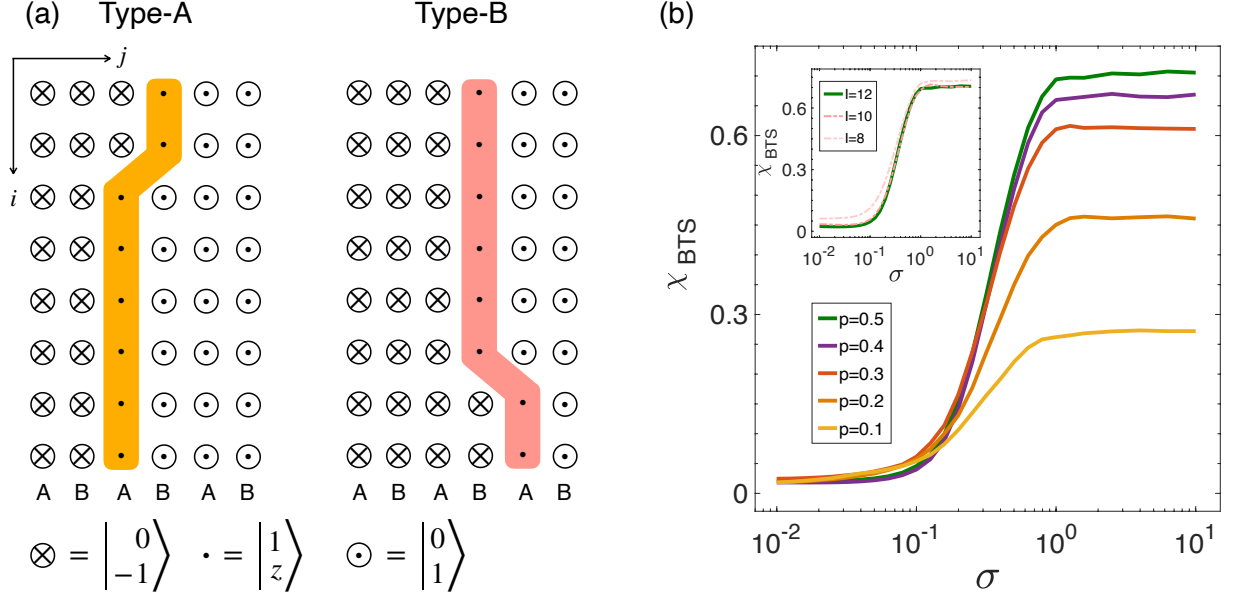


FIG. 2. Quantum peratic phase transition. (a), schematic illustration of the frustration free quantum system. The model contains a 2d array of qudits having a local four-dimensional Hilbert space. The legal quantum states correspond to the two types of line configurations shown in this plot (*see the description in the main text*). (b), the BTS response across the quantum peratic phase transition. Here we sample the surface terms h_{surf} with different p values from 0.1 to 0.5. The quantum ground state phase transition as constructed is dual to the quantum ergodic to many-body-localized dynamical phase transition. At weak disorder (small σ), the bulk is robust against surface manipulations giving a vanishing BTS, which is dual to the dynamical quantum ergodic phase. At strong disorder, the bulk is stringently tied with surface, corresponding to the dynamical many-body localized phase. The inset of (b) shows the system size dependence of BTS response (with p fixed at 0.5), which indicates the phase transition becomes sharper at larger system size.

$e^{-i(\hat{z}_i \hat{z}_{i+1} / 10 + \delta_i \hat{z}_i)}$ from $l = 4l$ to $6l - 1$. This unitary update process is then repeated forward for $J/6$ periods. The amplitude δ_i is a random number drawn from a Gaussian distribution with zero mean and variance σ^2 .

The constructed 2d local qudit Hamiltonian is semi-positive definite and frustration free [34], whose ground state is $|G(\vec{z}_\star)\rangle = \frac{1}{\sqrt{2^l}} \sum_l |\gamma_l(\vec{z}_\star)\rangle$, having a 2^l -fold degeneracy as labeled by \vec{z}_\star . The ground state is an equal-probability quantum superposition of those geometrical line configurations in Fig. 2.

We introduce a bulk observable to diagnose the peratic phase transition,

$$O_{ij} = \left| \begin{array}{c} 1 \\ 1 \end{array} \right\rangle \left\langle \begin{array}{c} 1 \\ 1 \end{array} \right| - \left| \begin{array}{c} 1 \\ -1 \end{array} \right\rangle \left\langle \begin{array}{c} 1 \\ -1 \end{array} \right|, \quad (8)$$

that acts on the site (i, j) . The ground state degeneracy would be lifted up by adding a perturbation on the edge $\Delta H = \sum_i h_{\text{surf}}^{[i]} [1 - O_{i,0}]$ —different choices of h_{surf} select ground states $|G(\vec{z}_\star)\rangle$ with different \vec{z}_\star . The corresponding BTS response is

$$\chi_{\text{BTS}} = \lim_{h_{\text{surf}} \rightarrow 0} \left[\frac{1}{I} \sum_{ij} \left(\overline{\langle O_{ij} \rangle^2} - \overline{\langle O_{ij} \rangle}^2 \right) \Big|_{h_{\text{surf}}} \right],$$

which is given by $\chi_{\text{BTS}} = \frac{1}{J^2} \sum_{i,l} \left\{ \overline{(\sum_{\vec{z}} z_i |\psi_l(\vec{z})|^2)^2} - (\overline{\sum_{\vec{z}} z_i |\psi_l(\vec{z})|^2})^2 \right\}$, with $\overline{\dots}$ averaging over different \vec{z}_\star . Treating unitary update from l to $l+1$

as quantum time evolution, the dynamics of $\psi_l(\vec{z})$ has two distinctive phases—quantum ergodic and MBL. For the MBL dynamics, the wave function holds the memory of the initial configuration of \vec{z}_\star , and the resultant BTS response χ_{BTS} of the dual 2d quantum ground state is finite, and strongly depends on \vec{z}_\star , namely the p -value in sampling $h_{\text{surf}}^{[i]}$. On the contrary for the quantum ergodic dynamics, the local observables would thermalize as l proceeds and are then independent of \vec{z}_\star , rendering a vanishing BTS response for the 2d ground state. The numerical results are provided in Fig. 2(b), which agree well with the theoretical analysis. The BTS response thus defines a peratic quantum phase transition in the frustration free quantum ground states.

With the exact construction presented above and the numerical results for the transverse field Ising model (Supplementary Materials), we expect the quantum peratic phase transition to be generic, not relying on the duality with the quantum MBL to ergodic phase transition. This unconventional phase transition defined by bulk-to-surface response could arise in a broad range of quantum simulation platforms as well as anisotropic spin glass materials.

Conclusion and Outlook.— We have discovered a peratic phase transition defined by a bulk-to-surface response in both classical and quantum ground states, which reaches beyond conventional phase transition paradigms. By constructing frustration free models, we establish rigorous duality from the peratic phase transition to order-to-chaos transition in the clas-

sical system, and to MBL-to-ergodic transition in the quantum setting. With numerical results, we show the peratic phase transition also preserves in frustrated Ising models, which describe a broad range of spin systems. As a specific example, we predict a system of Rydberg p-wave dressed atoms exhibits the peratic phase transition by tuning the interaction range. Our results indicate that dynamical phase transitions would inspire exotic phase transitions in equilibrium systems rather than reaching beyond.

Our construction of duality from dynamical phases to static Hamiltonian ground states is quite generic (Supplementary Materials). Given an arbitrary nonlinear dynamics of binary variables, the corresponding Hamiltonian can be systematically constructed. The Hamiltonian form for universal classical nonlinear dynamics is provided in Supplementary Materials. For quantum dynamics, we show as an example that the time crystal phase transition can be mapped to a static quantum phase transition. How to formulate the anomalous topological physics in Floquet quantum dynamics [17–19] in this framework is worth future investigation. Our approach provides an alternative way for characterizing dynamical phase transitions from the perspective of equilibrium phase transitions, which could unify the description of non-equilibrium phases within the equilibrium framework.

Acknowledgement.— We would like to thank Wei Wang for suggesting the ancient Greek “péras” for naming the phase transition, and thank Dong-Ling Deng for helpful discussion. This work is supported by National Natural Science Foundation of China (Grants No. 11774067, and 11934002), National Program on Key Basic Research Project of China (Grant No. 2017YFA0304204), Shanghai Municipal Science and Technology Major Project (Grant No. 2019SHZDZX01), Shanghai Science Foundation (Grant No. 21QA1400500, 19ZR1471500). Xingze Qiu acknowledges support from National Postdoctoral Program for Innovative Talents of China under Grant No. BX20190083.

* xiaopeng_li@fudan.edu.cn

- [1] L. D. Landau, On the theory of phase transitions. I., *Zh. Eksp. Teor. Fiz.* **11**, 19 (1937).
- [2] S. Weinberg, *The quantum theory of fields*, Vol. 2 (Cambridge university press, 1995).
- [3] M. Z. Hasan and C. L. Kane, Colloquium: Topological insulators, *Rev. Mod. Phys.* **82**, 3045 (2010).
- [4] X.-L. Qi and S.-C. Zhang, Topological insulators and superconductors, *Rev. Mod. Phys.* **83**, 1057 (2011).
- [5] X.-G. Wen, Colloquium: Zoo of quantum-topological phases of matter, *Rev. Mod. Phys.* **89**, 041004 (2017).
- [6] J. Demsar, Non-equilibrium phenomena in superconductors probed by femtosecond time-domain spectroscopy, *J. Low Temp. Phys.* **201**, 676 (2020).
- [7] M. Schreiber, S. S. Hodgman, P. Bordia, H. P. Lüschen, M. H. Fischer, R. Vosk, E. Altman, U. Schneider, and I. Bloch, Observation of many-body localization of interacting fermions in a quasirandom optical lattice, *Science* **349**, 842 (2015).
- [8] S. Deng, Z.-Y. Shi, P. Diao, Q. Yu, H. Zhai, R. Qi, and H. Wu, Observation of the efimovian expansion in scale-invariant fermi gases, *Science* **353**, 371 (2016).
- [9] J. Smith, A. Lee, P. Richerme, B. Neyenhuis, P. W. Hess, P. Hauke, M. Heyl, D. A. Huse, and C. Monroe, Many-body localization in a quantum simulator with programmable random disorder, *Nature Physics* **12**, 907 (2016).
- [10] S. Choi, J. Choi, R. Landig, G. Kucsko, H. Zhou, J. Isoya, F. Jelezko, S. Onoda, H. Sumiya, V. Khemani, *et al.*, Observation of discrete time-crystalline order in a disordered dipolar many-body system, *Nature* **543**, 221 (2017).
- [11] J. Zhang, P. Hess, A. Kyprianidis, P. Becker, A. Lee, J. Smith, G. Pagano, I.-D. Potirniche, A. C. Potter, A. Vishwanath, *et al.*, Observation of a discrete time crystal, *Nature* **543**, 217 (2017).
- [12] P. Roushan, C. Neill, J. Tangpanitanon, V. M. Bastidas, A. Megrant, R. Barends, Y. Chen, Z. Chen, B. Chiaro, A. Dunsworth, *et al.*, Spectroscopic signatures of localization with interacting photons in superconducting qubits, *Science* **358**, 1175 (2017).
- [13] Z. Yan, Y.-R. Zhang, M. Gong, Y. Wu, Y. Zheng, S. Li, C. Wang, F. Liang, J. Lin, Y. Xu, *et al.*, Strongly correlated quantum walks with a 12-qubit superconducting processor, *Science* **364**, 753 (2019).
- [14] K. Xu, Z.-H. Sun, W. Liu, Y.-R. Zhang, H. Li, H. Dong, W. Ren, P. Zhang, F. Nori, D. Zheng, *et al.*, Probing dynamical phase transitions with a superconducting quantum simulator, *Science Advances* **6**, eaba4935 (2020).
- [15] R. Nandkishore and D. A. Huse, Many-body localization and thermalization in quantum statistical mechanics, *Ann. Rev. Cond. Matt. Phys.* **6**, 15 (2015).
- [16] D. A. Abanin, E. Altman, I. Bloch, and M. Serbyn, Colloquium: Many-body localization, thermalization, and entanglement, *Rev. Mod. Phys.* **91**, 021001 (2019).
- [17] T. Kitagawa, E. Berg, M. Rudner, and E. Demler, Topological characterization of periodically driven quantum systems, *Phys. Rev. B* **82**, 235114 (2010).
- [18] L. Jiang, T. Kitagawa, J. Alicea, A. R. Akhmerov, D. Pekker, G. Refael, J. I. Cirac, E. Demler, M. D. Lukin, and P. Zoller, Majorana fermions in equilibrium and in driven cold-atom quantum wires, *Phys. Rev. Lett.* **106**, 220402 (2011).
- [19] M. S. Rudner, N. H. Lindner, E. Berg, and M. Levin, Anomalous edge states and the bulk-edge correspondence for periodically driven two-dimensional systems, *Phys. Rev. X* **3**, 031005 (2013).
- [20] A. Shapere and F. Wilczek, Classical time crystals, *Phys. Rev. Lett.* **109**, 160402 (2012).
- [21] F. Wilczek, Quantum time crystals, *Phys. Rev. Lett.* **109**, 160401 (2012).
- [22] V. Khemani, A. Lazarides, R. Moessner, and S. L. Sondhi, Phase structure of driven quantum systems, *Phys. Rev. Lett.* **116**, 250401 (2016).
- [23] D. V. Else, B. Bauer, and C. Nayak, Floquet time crystals, *Phys. Rev. Lett.* **117**, 090402 (2016).
- [24] J. Kelso, A. Mandell, and M. Shlesinger, *Dynamic Patterns in Complex Systems* (World Scientific, 1988) Chap. Adaptation toward the edge of chaos, pp. 293–301.
- [25] J. M. Deutsch, Quantum statistical mechanics in a closed system, *Phys. Rev. A* **43**, 2046 (1991).
- [26] M. Srednicki, Chaos and quantum thermalization, *Phys. Rev. E* **50**, 888 (1994).
- [27] M. Rigol, V. Dunjko, and M. Olshanii, Thermalization and its mechanism for generic isolated quantum systems, *Nature* **452**, 854 (2008).
- [28] N. Bertschinger and T. Natschläger, Real-Time Computation at

- the Edge of Chaos in Recurrent Neural Networks, *Neural Computation* **16**, 1413 (2004).
- [29] M. Saffman, T. G. Walker, and K. Mølmer, Quantum information with rydberg atoms, *Rev. Mod. Phys.* **82**, 2313 (2010).
- [30] M. Kjaergaard, M. E. Schwartz, J. Braumüller, P. Krantz, J. I.-J. Wang, S. Gustavsson, and W. D. Oliver, Superconducting qubits: Current state of play, *Ann. Rev. Cond. Matt. Phys.* **11**, 369 (2020).
- [31] K. Binder and A. P. Young, Spin glasses: Experimental facts, theoretical concepts, and open questions, *Rev. Mod. Phys.* **58**, 801 (1986).
- [32] J. Z. Imbrie, On many-body localization for quantum spin chains, *J. Stat. Phys.* **163**, 998 (2016).
- [33] P. Ponte, Z. Papić, F. m. c. Huveneers, and D. A. Abanin, Many-body localization in periodically driven systems, *Phys. Rev. Lett.* **114**, 140401 (2015).
- [34] A. Y. Kitaev, A. Shen, M. N. Vyalyi, and M. N. Vyalyi, *Classical and quantum computation* (American Mathematical Soc., 2002).

Supplementary Material: Peratic Phase Transition by Bulk-to-Surface Response

Xingze Qiu,^{1,2} Hai Wang,^{1,2} Wei Xia,¹ and Xiaopeng Li^{1,2,*}

¹*State Key Laboratory of Surface Physics, Institute of Nanoelectronics and Quantum Computing,
and Department of Physics, Fudan University, Shanghai 200438, China*

²*Shanghai Qi Zhi Institute, Shanghai 200030, China*

(Dated: September 29, 2021)

PHENOMENOLOGICAL THEORY AND SCALING ANALYSIS

To analyze the peratic phase transition, we propose a phenomenological theory and perform scaling analysis. Since the bulk-to-surface (BTS) response that characterizes the phase transition also probes the degree of fluctuations in the bulk system, resembling the entropy, the phenomenological free energy near the phase transition takes a form of

$$f(t, \chi_{\text{BTS}}) = -r(t)\chi_{\text{BTS}} + \kappa(t)\chi_{\text{BTS}}^2 + \mathcal{O}(\chi_{\text{BTS}}^3), \quad (\text{S1})$$

where we have $t = (\sigma - \sigma_c)/\sigma_c$, $r > 0$ ($r < 0$) for $t > 0$ ($t < 0$), and $\kappa > 0$. This free energy does not have Ising symmetry. Nonetheless, minimizing the free energy under the physical constraint $\chi_{\text{BTS}} \geq 0$ produces a phase transition, i.e., the peratic phase transition established in the main text.

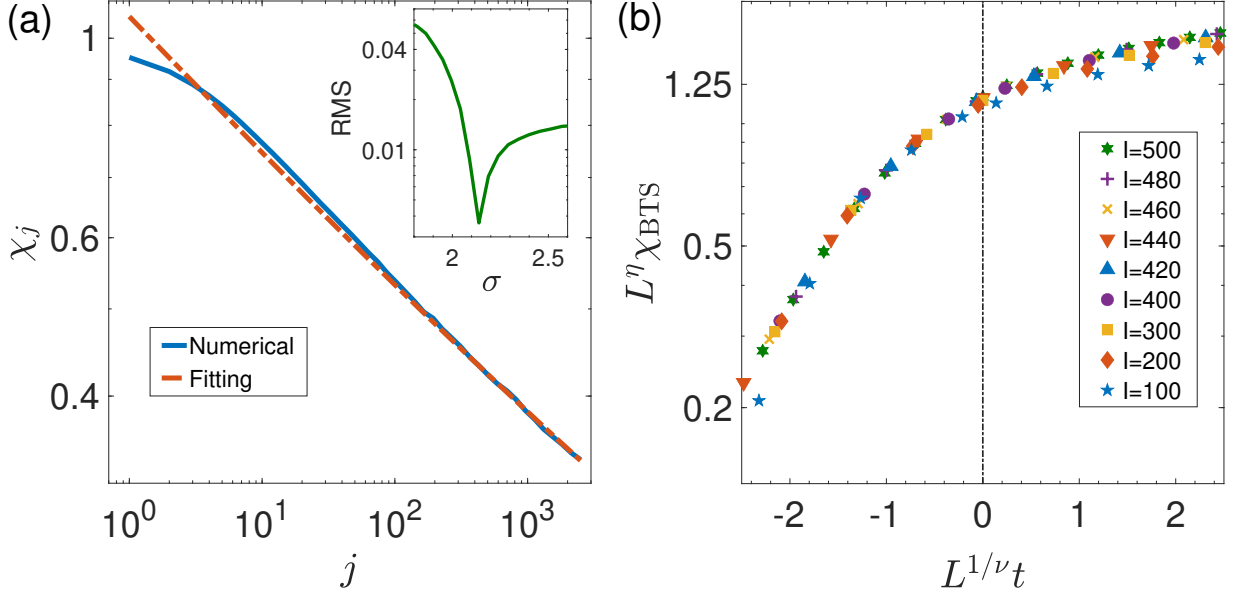


FIG. S1. Finite size scaling analysis for the classical peratic phase transition. (a), power law decay of the local bulk-to-surface (BTS) response in χ_j and the η -exponent. This exponent is obtained by fitting our numerical results for χ_j to a power law at the critical point. The inset shows the RMS error for fitting χ_j near the critical point to a power law function, and the location of the minimum indicates the critical point. In this plot, we choose $I = 500$, $J = 5I$, and $M = 2$. The η exponent is obtained to be $0.172(2)$. (b), data collapse in the scaling analysis for the BTS response. Here, we choose $M = 2$, $L = I$, $J = 5I$. In (b), we take $\nu = 2.732$, which gives the best-quality data collapse.

The scaling analysis is performed by postulating the phase transition is described by a certain renormalization group fixed point [1]. Taking a renormalization group transformation, $t \rightarrow t\zeta^{1/\nu}$, $L \rightarrow L/\zeta$ (the system size $I, J \propto L$), with ζ a scaling factor, and ν a critical exponent, we have

$$\chi_{j/\zeta}(t\zeta^{1/\nu}, L/\zeta) = \zeta^\eta \chi_j(t, L), \quad (\text{S2})$$

at the neighborhood of the fixed point. Here, η is the anomalous dimension. The ν and η exponents are to be fixed with our numerical results. The scaling form implies that

$$\chi_j(t, L) = j^{-\eta} A(jt^\nu, Lt^\nu), \quad (\text{S3})$$

with $A(\dots)$ a universal function. It then follows directly that a thermodynamic limit system right at the peratic phase transition point has a power law local BTS response,

$$\chi_j \propto j^{-\eta}. \quad (\text{S4})$$

The scaling of the total BTS response obeys

$$\chi_{\text{BTS}}(t\zeta^{1/\nu}, L/\zeta) = \zeta^\eta \chi_{\text{BTS}}(t, L), \quad (\text{S5})$$

which implies

$$\chi_{\text{BTS}}(t, L) = L^{-\eta} G(Lt^\nu), \quad (\text{S6})$$

with $G(\dots)$ a universal function.

The η -exponent is determined by fitting our numerical results to $\chi_j \propto j^{-\eta}$ at the critical point (Fig. S1(a)), from which we get $\eta = 0.172(2)$. We first fit all numerical results near the critical point for χ_j to a power law, and locate the critical point by minimizing the root mean square (RMS) error of the fitting. The value of the η -exponent and its error are obtained by fitting the data right at the critical point.

The ν -exponent is extracted by performing a data collapse taking the scaling form in Eq. (S6) (Fig. S1(b)), and we get $\nu = 2.73(8)$. The ν exponent is calculated using the analysis in Ref. [2], with the error estimated by bootstrap.

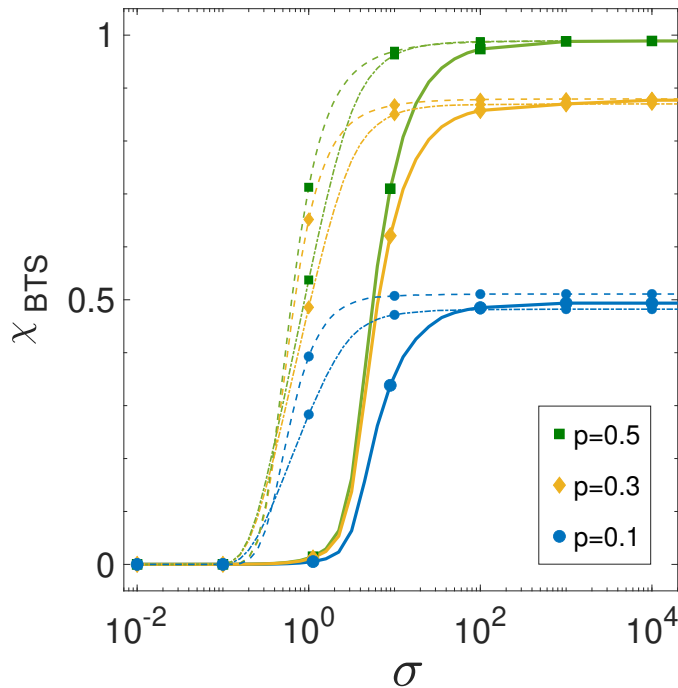


FIG. S2. The peratic phase transition in the frustrated Ising model [Eq. (6) *in the main text*]. The BTS response is averaged over different surface terms, with $p = 0.1, 0.3, 0.5$. The dashed lines show the results of the frustration free model [Eq. (2) *in the main text*] for comparison. The solid and dash-dotted lines correspond to the frustrated Ising model with and without transverse field, respectively. We choose a transverse field strength $h_T = 10$. In this plot, we choose $I = 5$, $J = 5$, and $M = 2$.

NUMERICAL RESULTS FOR THE EXPERIMENTAL CANDIDATES

For experimental candidates, we have considered Hamiltonians with two-body Ising couplings [see Eq. (6) and the subsequent discussion *in the main text*]. Here, we show the numerical results in Fig. S2. We observe that the BTS responses for the frustrated and frustration-free models are quite similar to each other with a tiny difference barely noticeable. Besides, the peratic phase transition still persists in presence of quantum fluctuations. We find quantum fluctuations further stabilize the rigid phase and shift the transition point towards the volatile phase, which is somewhat counterintuitive. This can be attributed to that the transverse field couples the degenerate ground states and develops a tendency for gap opening, rendering the bulk more rigid. As a specific example, we consider a system of Rydberg p -wave dressed atoms in the following section.

PERATIC PHASE TRANSITION IN RYDBERG ATOMIC ARRAYS

Given the programmable quantum annealing architectures [3, 4], all Ising models can be experimentally implemented with Rydberg atoms. In this section, we discuss the actual realization of the peratic phase transition is less demanding

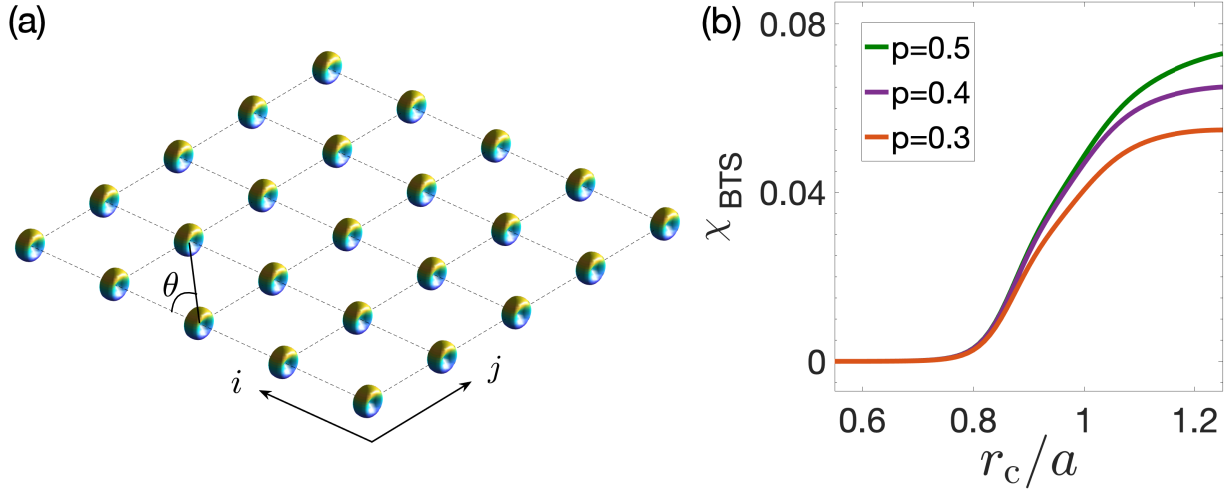


FIG. S3. Peratic phase transition with Rydberg atom arrays. (a), schematic illustration of the Rydberg atom arrays. The atoms are dressed to a Rydberg p -wave state and located on a 2D square lattice, whose lattice constant is a . (b), the BTS response across the peratic phase transition. The strength of longitudinal fields are fixed along the i -axis, and random drawn from the binary values $\pm V$ with equal probability along the j -axis. The BTS response is averaged over all configurations of the different longitudinal fields and different surface terms, with $p = 0.3, 0.4, 0.5$. Here, we set the transverse field strength $h_T = 0.5V$, and the system size as 5×5 .

than reaching universal quantum annealing. We consider a system of Rydberg p -wave dressed atoms, which has been used to construct quantum spin ice Hamiltonians [5] and programmable quantum annealing [4]. In this system, the two binary degrees of freedom ($|\uparrow\rangle$, and $|\downarrow\rangle$) correspond to two atomic hyperfine states $|5^2S_{1/2}, F=2, m_F=0\rangle$ and $|5^2S_{1/2}, F=1, m_F=0\rangle$ of ^{87}Rb atoms. Taking a Rydberg p -wave dressing scheme where the $|\uparrow\rangle$ state is selectively dressed with a Rydberg p -wave state $|n^2P_{3/2}, m=3/2\rangle$ (the quantization axis along the i -direction in Fig. S3), we introduce interactions between neighboring layers as labeled by j , without intra-layer couplings for the symmetry properties of Rydberg p -wave interaction [5]. Arranging the atoms periodically in a 2d array (Fig. S3), the resultant interaction between the two qubits at \vec{r} and \vec{r}' is given by

$$H_1 = \sum_{\vec{r}, \vec{r}'} \frac{V \sin^4 \theta_{\vec{r}\vec{r}'}}{1 + \left(\frac{|\vec{r}-\vec{r}'|}{r_c}\right)^6} (\hat{z}_{\vec{r}} + 1)(\hat{z}_{\vec{r}'} + 1)/2, \quad (\text{S7})$$

with the coupling strength V and the characteristic interaction range r_c determined by the Rabi frequency and the detuning of the one-photon transition of the Rydberg dressing scheme [5].

With the Rydberg setup, the transverse field can be induced by performing a microwave induced transition between the two hyperfine states, described by a Hamiltonian

$$H_2 = \sum_{\vec{r}} h_T \hat{x}_{\vec{r}}, \quad (\text{S8})$$

with h_T fixed by the Rabi frequency of the microwave coupling. The on-site longitudinal field is tunable by manipulating the detuning of the microwave with respect to the hyperfine splitting of 6.8 GHz. The longitudinal fields are described by

$$H_3 = \sum_{\vec{r}} h_{\vec{r}} \hat{z}_{\vec{r}}. \quad (\text{S9})$$

The realized Hamiltonian closely resembles the anisotropic Ising model studied in the main text, which exhibits a peratic phase transition.

Here, we carry out ground state calculation for the system of Rydberg dressed atoms directly. Fig. S3 shows the results. When the interaction range r_c is much smaller than the lattice spacing, the system is weakly coupled, for

which the ground state is in a rigid phase with vanishing bulk-to-surface response. The corresponding spin polarization is fixed by the local detuning. By increasing the interaction range, we find that the peratic phase transition happens, and the system is driven towards the volatile phase, with finite bulk-to-surface response.

MAPPING BINARY VARIABLE DYNAMICS TO HAMILTONIAN GROUND STATES

We consider a generic dynamical evolution of a binary sequence $\mathbf{z}_t \equiv [z_{0,t}, z_{1,t}, \dots, z_{I-1,t}]^T$ (a column vector), with t the evolution time. A generic binary variable dynamics is described by a dynamical equation,

$$\mathbf{z}_t = \text{sgn}(F_t(\mathbf{z}_{t-1})), \quad (\text{S10})$$

with F_t an arbitrary function. A Turing complete binary circuit can also be formulated in this form. The time-evolved configuration is the ground state of a static Hamiltonian,

$$H = - \sum_t \mathbf{z}_t^T \text{sgn}(F_t(\mathbf{z}_{t-1})), \quad (\text{S11})$$

by treating t as a real space column index. The solution existence of Eq. (S10) guarantees the Hamiltonian ground state is frustration free. If we further impose a local constraint on the binary variable dynamics, namely assuming $z_{i,t}$ is determined by its neighboring binary variables $z_{i' \in [i-M, i+M], t-1}$ only (M is a finite number), the local dynamical equation takes a form

$$z_{i,t} = \text{sgn} [F_{i,t}(\{z_{i' \in [i-M, i+M], t-1}\})]. \quad (\text{S12})$$

The Hamiltonian in Eq. (S11) is then reduced to

$$H = - \sum_{i,t} z_{i,t} \text{sgn} [F_{i,t}(\{z_{i' \in [i-M, i+M], t-1}\})], \quad (\text{S13})$$

which only contains local couplings on a 2d grid. We thus conclude generic local Ising variable dynamics can be mapped to ground states of a local Hamiltonian. We expect this holds for arbitrary dynamical evolution in discrete settings, for that the discrete degrees of freedom can be rigorously encoded by Ising variables.

CONSTRUCTION OF A FRUSTRATION FREE QUANTUM MODEL

We consider a 2d array of qudits. Its Hilbert space is projected to a low-energy subspace by introducing an energy penalty

$$H_P = \lambda (P_1 + P_2 + P_3 + P_4),$$

with $P_{1,2,3,4}$ four local projectors as described below. The projector P_1 acts on columnwise nearby sites (i, j) , and $(i+1, j)$ (see Fig. 3 in the main text for illustration),

$$P_1 = \sum_{zz'} \left[\sum_{i,j \in A} \begin{vmatrix} 1 & 0 \\ z & z' \end{vmatrix} \begin{vmatrix} 1 & 0 \\ z & z' \end{vmatrix} + \sum_{i,j \in B} \begin{vmatrix} 0 & 1 \\ z & z' \end{vmatrix} \begin{vmatrix} 0 & 1 \\ z & z' \end{vmatrix} \right].$$

The projectors P_2 and P_3 both act on rowwise nearby sites (i, j) and $(i, j+1)$,

$$P_2 = \sum_{ij} \left[\sum_{zz'} \begin{vmatrix} 1 & 1 \\ z & z' \end{vmatrix} \begin{vmatrix} 1 & 1 \\ z & z' \end{vmatrix} + \begin{vmatrix} 0 & 0 \\ 1 & -1 \end{vmatrix} \begin{vmatrix} 0 & 0 \\ 1 & -1 \end{vmatrix} \right],$$

$$P_3 = \sum_{ij} \left[\sum_z \begin{vmatrix} 1 & 0 \\ z & -1 \end{vmatrix} \begin{vmatrix} 1 & 0 \\ z & -1 \end{vmatrix} + \begin{vmatrix} 0 & 1 \\ 1 & z \end{vmatrix} \begin{vmatrix} 0 & 1 \\ 1 & z \end{vmatrix} \right].$$

The projector P_4 contains four-body interactions acting on the sites $\{(i, j-1), (i, j), (i, j+1), (i \pm 1, j)\}$,

$$P_4 = \sum_{ij} \sum_{z_1 z_2 z_3 z_4} \left| \begin{array}{cccc} 0 & 0 & 0 & 1 \\ z_1 & z_2 & z_3 & z_4 \end{array} \right\rangle \left\langle \begin{array}{cccc} 0 & 0 & 0 & 1 \\ z_1 & z_2 & z_3 & z_4 \end{array} \right|.$$

The low energy legal subspace ($|\text{Legal}\rangle$) is defined by $P_{1,2,3,4}|\text{Legal}\rangle = 0$. The legal quantum states in the subspace correspond to line configurations as shown in Fig. 3 (*the main text*). We assume the strength of the energy penalty λ is large enough to suppress all possible fluctuations leaving the subspace.

We now construct a microscopic local Hamiltonian that produces the effective Hamiltonian for legal quantum states in Eq. (7) (*main text*). The microscopic Hamiltonian takes a form,

$$H = \sum_{i,j \in A} H_{ij}^A + \sum_{i,j \in B} H_{ij}^B \quad (\text{S14})$$

with H_{ij}^A and H_{ij}^B three-local interactions acting on the sites $\{(ij), (i+1, j), (i, j+1)\}$, and $\{(i-1, j), (i, j), (i, j+1)\}$, respectively, defined by

$$\begin{aligned} H_{ij}^A &= \sum_{z_1 z_2} \left| \begin{array}{ccc} 0 & 1 & 1 \\ -1 & z_1 & z_2 \end{array} \right\rangle \left\langle \begin{array}{ccc} 0 & 1 & 1 \\ -1 & z_1 & z_2 \end{array} \right| \\ &\quad - \frac{1}{2} \sum_{z_1, 2, z'_1, 2} \left[U_{z_1 z_2; z'_1 z'_2}^{[ij]} \left| \begin{array}{ccc} 0 & 1 & 1 \\ -1 & z_2 & z_1 \end{array} \right\rangle \left\langle \begin{array}{ccc} 1 & 1 & 0 \\ z'_1 & z'_2 & 1 \end{array} \right| + H.c. \right], \\ H_{ij}^B &= \sum_{z_1 z_2} \left| \begin{array}{ccc} 1 & 0 & 1 \\ z_1 & -1 & z_2 \end{array} \right\rangle \left\langle \begin{array}{ccc} 1 & 0 & 1 \\ z_1 & -1 & z_2 \end{array} \right| \\ &\quad - \frac{1}{2} \sum_{z_1, 2, z'_1, 2} \left[U_{z_1 z_2; z'_1 z'_2}^{[ij]} \left| \begin{array}{ccc} 1 & 0 & 1 \\ z_1 & -1 & z_2 \end{array} \right\rangle \left\langle \begin{array}{ccc} 1 & 1 & 0 \\ z'_1 & z'_2 & 1 \end{array} \right| + H.c. \right]. \end{aligned}$$

The interaction elements $U_{z_1 z_2; z'_1 z'_2}^{[ij]}$ form a unitary matrix, with $\sum_{z_1 z_2} U_{z'_1 z'_2; z_1 z_2}^{[ij]} U_{z_1 z_2; z'_1 z'_2}^{[ij]*} = \delta_{z'_1 z'_1} \delta_{z'_2 z'_2}$. Projecting the microscopic Hamiltonian to the legal subspace, we reach the effective Hamiltonian provided in *the main text*, with the γ -states defined according to its wave function $\psi_l(\vec{z})$ by

$$\psi_{l_{ij}}(\vec{z}) = \sum_{z'_i z'_{i+1}} U_{z_i z_{i+1}; z'_i z'_{i+1}}^{[ij]} \psi_{l_{ij}-1}(z_0 \dots z_{i-1} z'_i z'_{i+1} \dots z_{I-1}).$$

The Hamiltonian is frustration free within the legal subspace. Taking l as a time step, the unitary update of $\psi_l(\vec{z})$ corresponds to unitary time evolution under a series of two-qubit gates defined by their matrix representation, $U^{[ij]}$. This Hamiltonian construction has been inspired by the geometrical Kitaev-Feynmann clock states, which have been used to prove the computational QMA-completeness of 2d quantum lattice models [6, 7].

THE EXACT GROUND STATE DUAL OF TIME CRYSTAL

In this section, we show that the non-equilibrium time crystal phase transition [8–13] also has an exact dual to a phase transition in the ground states of a static Hamiltonian. This Hamiltonian has the same form as that in Eq. (6) in the main text, but with the γ -states $|\gamma_l(\vec{z}_*)\rangle = \sum_{\vec{z}} \psi_l(\vec{z}) |l; \vec{z}\rangle$, updated in a different way. Here for the time crystal, we update the wave functions $\psi_l(\vec{z})$ through a Floquet time crystal dynamics of a one-dimensional (1d) spin-1/2 system [11]. From $l = 0$ to $l = I - 1$, the update of ψ_l corresponds to the unitary gates $e^{i\hat{x}_i h_x}$ (i from 0 to $I - 1$), and then the unitary gates $e^{-i(J^{[i]} \hat{z}_i \hat{z}_{i+1} + h_z^{[i]} \hat{z}_i + h_x^{[i]} \hat{x}_i)}$ (i from $I - 1$ to 0) are applied from $l = I$ to $2I - 1$. The amplitudes $J^{[i]}$, $h_z^{[i]}$, and $h_x^{[i]}$ are chosen from certain random distributions. This unitary update process is then repeated forward for $J/2$ periods.

In Section , we have constructed a 2d local qudit Hamiltonian, whose projection on the legal subspace gives the effective Hamiltonian and whose ground state $|G(\vec{z}_*)\rangle = \frac{1}{\sqrt{IJ}} \sum_l |\gamma_l(\vec{z}_*)\rangle$ encodes the whole Floquet quantum dynamics. From the construction, we observe that this local qudit Hamiltonian has lattice translation symmetry (LTS) along the j -axis, with A and B sites forming a sublattice structure. Note that this LTS is dual to the time-translation symmetry (TTS) of the Floquet quantum dynamics. The time crystal phase transition arising from TTS

breaking has an exact dual to the phase transition in the ground state $|G(\vec{z}_*)\rangle$ due to LTS breaking. The operator given in Eq. (8) *in the main text* also characterizes this symmetry breaking. The corresponding order parameter reads

$$C(O) = \frac{1}{I} \left[\sum_{i,j \in A} (-1)^{j/2} \langle G(\vec{z}_*) | O_{ij} | G(\vec{z}_*) \rangle \right]. \quad (\text{S15})$$

In the thermodynamic limit, this order parameter vanishes in the symmetric phase, and becomes finite in the LTS broken phase.

* xiaopeng_li@fudan.edu.cn

- [1] A. Altland and B. D. Simons, [Condensed matter field theory](#) (Cambridge university press, 2010).
- [2] S. M. Bhattacharjee and F. Seno, A measure of data collapse for scaling, [Journal of Physics A: Mathematical and General](#) **34**, 6375 (2001).
- [3] W. Lechner, P. Hauke, and P. Zoller, A quantum annealing architecture with all-to-all connectivity from local interactions, [Science Advances](#) **1**, e1500838 (2015).
- [4] X. Qiu, P. Zoller, and X. Li, Programmable quantum annealing architectures with ising quantum wires, [PRX Quantum](#) **1**, 020311 (2020).
- [5] A. W. Glaetzle, M. Dalmonte, R. Nath, I. Rousochatzakis, R. Moessner, and P. Zoller, Quantum spin-ice and dimer models with rydberg atoms, [Phys. Rev. X](#) **4**, 041037 (2014).
- [6] A. Y. Kitaev, A. Shen, M. N. Vyalyi, and M. N. Vyalyi, [Classical and quantum computation](#) (American Mathematical Soc., 2002).
- [7] D. Aharonov, W. van Dam, J. Kempe, Z. Landau, S. Lloyd, and O. Regev, Adiabatic quantum computation is equivalent to standard quantum computation, [SIAM Journal on Computing](#) **37**, 166 (2007).
- [8] A. Shapere and F. Wilczek, Classical time crystals, [Phys. Rev. Lett.](#) **109**, 160402 (2012).
- [9] F. Wilczek, Quantum time crystals, [Phys. Rev. Lett.](#) **109**, 160401 (2012).
- [10] V. Khemani, A. Lazarides, R. Moessner, and S. L. Sondhi, Phase structure of driven quantum systems, [Phys. Rev. Lett.](#) **116**, 250401 (2016).
- [11] D. V. Else, B. Bauer, and C. Nayak, Floquet time crystals, [Phys. Rev. Lett.](#) **117**, 090402 (2016).
- [12] J. Zhang, P. Hess, A. Kyprianidis, P. Becker, A. Lee, J. Smith, G. Pagano, I.-D. Potirniche, A. C. Potter, A. Vishwanath, et al., Observation of a discrete time crystal, [Nature](#) **543**, 217 (2017).
- [13] S. Choi, J. Choi, R. Landig, G. Kucsko, H. Zhou, J. Isoya, F. Jelezko, S. Onoda, H. Sumiya, V. Khemani, et al., Observation of discrete time-crystalline order in a disordered dipolar many-body system, [Nature](#) **543**, 221 (2017).